LETTER TO THE EDITOR

Three-dimensional magnetic resonance imaging of a liquid foam

Burkhard A Prause†, James A Glazier†, Samuel J Gravina‡ and Carlo D Montemagno§

† Department of Physics, University of Notre Dame, Notre Dame, IN 46556-5670, USA
‡ Bruker Instruments Inc., Billerica, MA 01821, USA
§ Department of Agricultural and Biological Engineering, Cornell University, Ithaca, New York 14853, USA

Abstract. We describe three-dimensional magnetic resonance imaging (MRI) of a liquid foam. Difficulties in imaging arise from the rate of evolution of the foam and the magnetic susceptibility mismatch at the boundaries between liquid and air. We used a protein gelatin foam, for which we improved relaxation rates and matched the susceptibility. A three-dimensional spin-echo sequence yielded strongly T_2 weighted signals. The reconstructed data represents the first such full three-dimensional image of a liquid foam.

Direct experimental measurement of the structure and evolution of a liquid three-dimensional foam requires a new, non-destructive technique to observe the foam's interior [1, 2]. Early topological results were obtained by Matzke in 1946 [3] and, more recently, Weaire and Phelan used optical microscopy to observe structures within, at most, a few layers of the surface in transparent dry foams [4]. Limited accuracy in determining depth makes it difficult to estimate volumes with this technique [5]. Durian, Weitz and Pine have observed a scaling state in a liquid foam using non-destructive diffusing light spectroscopy [6]. This approach is limited to measuring the average bubble diameter and does not allow studies of size distributions. The insertion probe techniques insert a narrow tube into each bubble, one at a time, to measure the volume of gas [7]. This technique provides a volume distribution, but destroys the sample and so cannot measure topology or time evolution.

Magnetic resonance imaging solves these problems, since it requires only the presence of polarizable protons in the sample. In principle, any sample containing ^{1}H (or any other suitable nucleus with non-zero spin) can be used for imaging. The signal intensity in a foam depends on the relative liquid content, since the gas inside the bubbles does not contribute to the signal. For wetness much less than the rigidity loss transition, where the foam is expected to possess an organized polyhedral structure, the liquid content is about 10%, making imaging difficult. Starting with a considerably wetter foam improves the signal. The quality of the image also depends on the rate of coarsening in the foam. A more slowly evolving foam allows longer aquisition times, increasing either the achievable signal to noise ratio or the resolution. Solid foams allow very long image aquisitions, but cannot show bubble evolution or drainage. Many froths evolve too rapidly for high resolution imaging. Clearly our ability to resolve bubbles depends on the particular choice of foam.

Hydrocarbon and water mixtures such as regular shaving cream evolve sufficiently slowly. Attempts by German and McCarthy to image bubbles in two-dimensional MRI of hydrocarbon foams such as egg white, cream and beer froth, did not resolve single

bubbles [8]. Gonatas *et al* have successfully imaged two-dimensional sections and obtained area distributions, but their apparatus was unable to achieve the necessary resolution along the third axis to acquire three-dimensional data [9].

We formed a protein solution from fish-skin-derived gelatin (Sigma Chemical, 45% aqueous teleostean gelatin). The presence of protein macro molecules (approximately 60 000 g mol^{-1}) reduces the amount of 'free' water, by binding water molecules to the protein. This binding creates two unique water phases. Both the longitudinal and the transverse relaxation rates for hydrogen in the bound water molecules are much higher than for unbound water. The total longitudinal relaxation time T_1 is inversely proportional to the fraction of bound water P_b [10, 11]. Decreasing the relative amount of water in the solution would have the desirable effect of aiding the realignment of the nuclear spins with the external magnetic field, enabling faster aquisition. However, protons contained in the α-amino-acids of proteins do not contribute to the nuclear magnetic resonance (NMR) signal, so that a high fraction of protein molecules diminishes the resonance intensity. We found a useful ratio to be 70% Sigma gelatin and 30% added water.

MRI samples that contain regions with different magnetic susceptibilities generate susceptibility artefacts. These artefacts are due to long-range field disturbances in the sample, that are created by induced magnetic dipoles at the boundaries between regions with different internal magnetic fields [12]. Since the oxygen in air is strongly paramagnetic, we carefully matched the susceptibility of the liquid to that of the air contained in the bubbles by adding a 15 mM concentration of Sigma DyTTHA-chelate to the solution. This paramagnetic chemical-shift agent nulled the localized field inhomogeneities and effectively reduced the signal linewidth. A 10 mM concentration of $CuSO_4$ served as a T_1 contrast agent, to reduce the longitudinal relaxation time by a factor of five [9].

We produced the foam by whipping the solution for about twenty minutes, using a commercial electric mixer. After whipping, the foam was allowed to drain for one hour, and was then carefully sucked into a 10 mm diameter syringe, to avoid trapping air. We used an optical microscope and CCD camera to study the distribution of bubble sizes in this foam, as well as the time scale and rate of drainage of liquid. These studies revealed that isolated, spherical bubbles remained suspended in the solution for several hours. Analysis of surface bubbles, within a region 3 mm to 10 mm above the level of drained liquid, showed that less than 35% of the bubbles were smaller than 200 μm after 90 min. Figure 1 shows that this fraction decreased steadily as the foam coarsened, and remained fairly constant at 15% to 20% in the foam's dry limit after ten hours. In order to obtain useful information about the shape of single bubbles, we require a minimum resolution of $4 \times 4 \times 4$ voxels per bubble, reducing the error due to the uncertainty in placing the boundaries between bubbles, which is of the order of one voxel. To avoid errors in the statistical size distribution we need to be able to resolve a known fraction of the bubbles in the sample. To exclude less than 35% of all bubbles, even at early stages of the foam's development, would require voxel dimensions of 50 μm in all directions, setting a lower bubble size cutoff of 200 μm.

The sample was less than two hours old at the time of imaging. Figure 2 shows the drained liquid volume measured during the first three hours. The high viscosity of the protein solution greatly reduces the flow rate compared to detergent-based foams. For more than two and a half hours the foam continues to drain at a largely constant rate. To perform MRI under conditions of continuing drainage, we needed to minimize the delocalization of spatially encoded molecules in the excited sample. To prevent distortions due to movement and coarsening of the suspended bubbles we needed to keep the total imaging time as short as possible, and we also needed short excitation times, coupled with strong dephasing gradients, to avoid artefacts from liquid flow along Plateau borders.
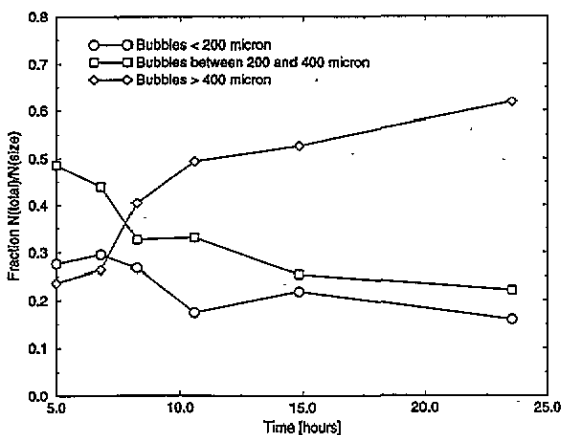
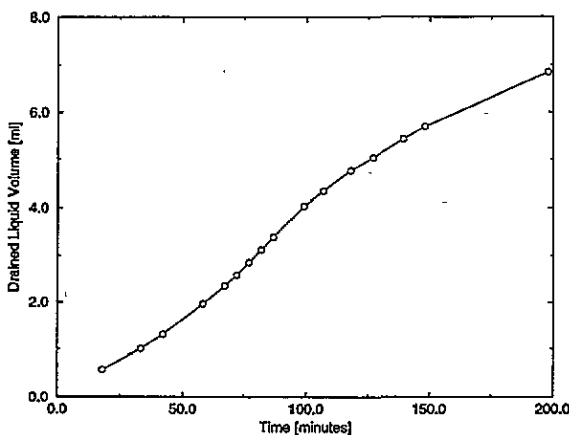**Figure 1.** Evolution of bubble diameter distributions between 5 and 24 hours.

Figure 2. Total volume of liquid drained from a 20 cm^3 foam sample over a period of three hours.

In the experiment we used a 9.4 T (400 MHz) Bruker AMX400 WB spectrometer, tuned to image protons. We set TR to 160 ms, 1.5 times the longitudinal relaxation time T_1, which maximizes the signal to noise ratio. TE was 868 μs to minimize image distortions due to remaining susceptibility variations in the sample. We used a 3D spin-echo sequence with $160 \times 160 \times 160$ samples collected in k-space.

The 3D spin-echo sequence phase encoded simultaneously in the x and z directions, while a horizontal read gradient was applied along the y axis. The sweep width across all 160 complex points was 125 kHz at a read gradient strength of 36.7 G cm^{-1}. The field of view was $8 \times 9.2 \times 8$ mm, yielding 100 μm resolution in the x and z directions and 115 μm along the y axis.

The digital resolution was enhanced by appending a zero fill of 48 points to the free induction decays (FID), giving us 128 real points along each axis. Two averages resulted in a 34 min aquisition time.

The analysis of the data focused on the full three-dimensional reconstruction of the image. In the analysis of foams we must not erode or dilate regions in the process of

improving the distinction between signal and background noise. In principle, the amount of information contained in the raw data cannot be improved. However, we can use advanced image processing techniques to eliminate random noise and sharpen existing edges. Thus we can more clearly seperate regions of different signal intensities, without shifting boundaries, and losing information about the original structure. For most of our analysis we used customized VoxelView 2.2 software and a Silicon Graphics Onyx workstation.

VoxelView calculates the relative signal to noise ratio, $S/N = \langle I \rangle + \sigma(I)$, where I is the normalized signal intensity of each voxel. In an average over all slices, the raw data possessed a very low relative S/N of 1.17.

We sectioned the data into 128 individual slices of 128 × 128 pixels each. First we applied an unsharp masking filter to sharpen the image. A 3 × 3 Laplacian operator creates smoothed ('out of focus') copies of the original slices, which are subtracted from the originals [13]. This filter suppresses gradual changes and passes high frequencies or edges, without shifting them. After filtering we reassembled the data into a three-dimensional array.

We then applied a neighbourhood ranking filter, which is a convolution operator that averages together pixels in a neighbourhood according to a defined weighting operation. We used a 3 × 3 × 3 uniform kernel, which assigns the largest value in the highest gradient direction to its centre element. This linear operation eliminates random noise without losing structural information [13]. The processed data possessed a respectable relative S/N of 1.90.

The experiment yields the first such three-dimensional image of a liquid foam.

Figure 3 is a surface rendering of the imaged volume. The cylindrical shape of the sample is apparent. The structure of single bubbles can be probed along any axis, as the cut section in the upper right demonstrates.
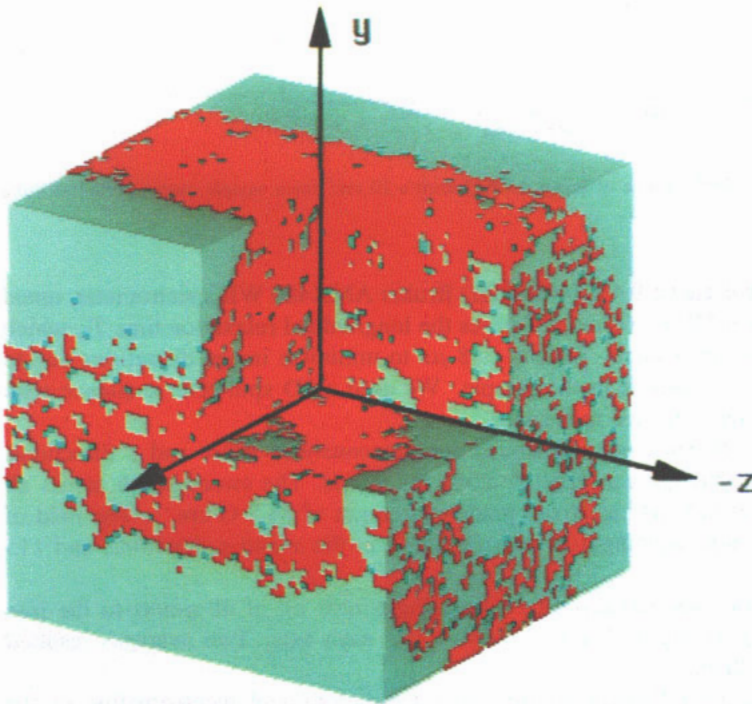

Figure 3. Surface rendering of the sample. Several slices are cut out to illustrate the 3d nature of the data.
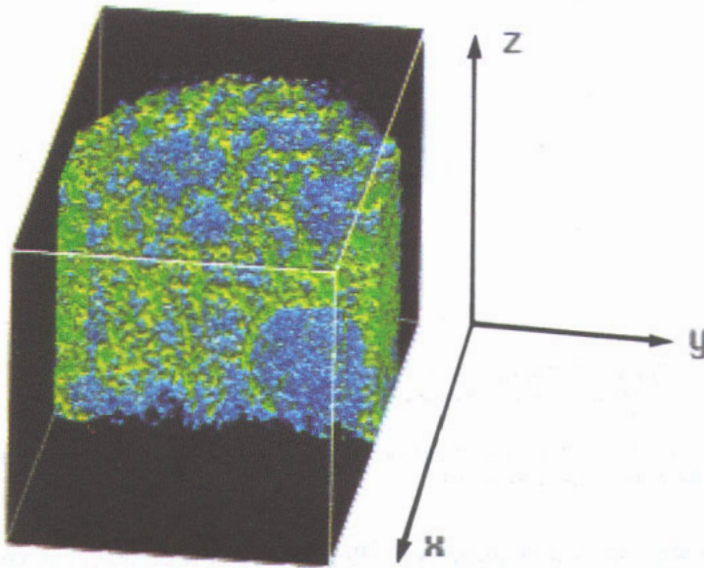
Figure 4. Three-dimensional image of the sample.

Figure 3, as well as figure 4 (a true three-dimensional image) shows the large proportion of water in the sample. Individual bubbles float in the solution and have not yet assumed polyhedral shapes. This result agrees with our optical studies that show isolated bubbles in the solution for up to ten hours. Bubbles accumulate at the bottom of the imaged volume. This area lies immediately above the liquid level of the sample, so that the accumulation occurs at a surprisingly sharp boundary between liquid foam and pure liquid. We analysed the liquid fraction $1 - \Phi$, Φ being the gas fraction, of our three-dimensional sample as a function of height above the drained liquid and found an oscillation of density near the liquid surface (figure 5). The result also appears to be present in the vertical wetness profile obtained by McCarthy [14]. To our knowledge McCarthy did not draw attention to this feature of his data, in which the liquid fraction of the foam oscillates near the liquid surface, as would be expected if the bubbles formed a few ordered layers at the boundary, as seen at vertical boundaries by Phelan and Weaire [4].

Two independent effects limit structural information about the bubbles. The average growth rate of bubbles at the limit of our resolution is very large. Studying the growth of individual bubbles with a microscope, we found their average diameter $\langle D_S(t = 90) \rangle$ after 90 min to be 150 μm. After 130 min we found $\langle D_S(t = 130) \rangle = 236$ μm. Thus the average volume of these bubbles doubles within twenty minutes. So, on average, the boundaries of individual bubbles at this size limit shift by more than one voxel during the imaging, decreasing the amount of spatial information by at least a factor of two. Flow of liquid also contributes to signal loss. The movement of molecules causes a loss of phase coherence and a delocalization of the resonance frequency during each excitation. We applied the read gradient horizontally to limit this effect. However, the flow through Plateau borders is three-dimensional, so we cannot entirely prevent a loss in signal quality.

MRI can resolve single bubbles in liquid foam in three dimensions and should be able to provide important information about the topological structure of a dry foam. A high initial water fraction that causes continuing rapid drainage, as well as movement and coarsening of the bubbles degrades the signal. More time for the foam to drain, longer aquisition times
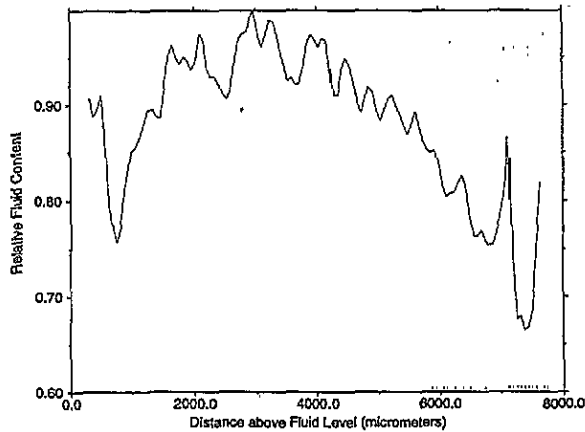
Figure 5. Relative water content in the sample as a function of height above the fluid level. We normalize the highest water content to 1.

and further optimization of the aquisition sequence will allow studies of time evolution and drainage in three dimensions.

References

[1] Glazier J A and Weaire D 1992 *J. Phys.: Condens. Matter* **4** 1867
[2] Glazier J A 1993 *Phys. Rev. Lett.* **70** 2170
[3] Matzke E B 1946 *Am. J. Bot.* **33** 58
[4] Weaire D and Phelan R 1994 *Phil. Mag. Lett.* **70** 345
[5] Williams W M and Smith C S 1952 *J. Met.* **194** 755
[6] Durian D J, Weitz D A and Pine D J 1990 *J. Phys.: Condens. Matter* **2** SA433
[7] Bisperink C G J, Akkerman J C, Prins A and Ronteltap A D 1992 *Food Struct.* **11** 101
[8] German J B and McCarthy M J 1989 *J. Agric. Food Chem.* **37** 1321
[9] Gonatas C P, Leigh J S, Yodh A G, Glazier J A and Prause B 1995 *Phys. Rev. Lett.* **75** 573
[10] Mansfield P and Morris P G 1982 1990 *NMR Imaging in Biomedicine: Supplement 2 Advances in Magnetic Resonance* (New York: Academic)
[11] Morris P G 1986 *Nuclear Magnetic Resonance in Medicine and Biology* (New York: Oxford University Press)
[12] Callaghan P T 1991 *Principles of Nuclear Magnetic Resonance Microscopy* (New York: Oxford University Press)
[13] Russ J C 1993 *The Image Processing Handbook* (Boca Raton, FL: Chemical Rubber Company)
[14] McCarthy M J 1990 *AIChE J.* **36** 287